Large-Scale Electromagnetic Field Analysis on Conductor Eddy Current Loss in Bar-Wound Coil Type Permanent Magnet Synchronous Motor for Automotive Applications

Masahiro Aoyama
Shizuoka University
3-5-1 Johoku, Naka-ku, Hamamatsu,
Shizuoka 432-8561, Japan
aoyama.masahiro@shizuoka.ac.jp

Deng Jianing, Yoshihiko Sunayama
SUZUKI Motor Corporation
300 Takatsuka-cho, Minami-ku,
Hamamatsu, Shizuoka 432-8611,Japan
Y. Sunayama : suna@hhq.suzuki.co.jp

Masahiko Miwa
JSOL Corporation
Tosabori Daibiru Bldg. 2-2-4 Tosabori,
Nishi-ku, Osaka 550-0001, Japan
miwa.masahiko@jsol.co.jp

***Abstract*—This paper describes a study of large-scale electromagnetic field analysis on super-computer (K-computer in Japan) in order to analyze the conductor eddy current loss of the interior permanent magnet synchronous motor using a bar-wound conductor in detail. In order to analyze the conductor eddy current loss due to the leakage magnetic flux at the typical driving point in detail, the same coil forming state as the actual prototype was modeled on the CAE and electromagnetic field analysis was performed. Furthermore, the preliminary study to reduce the conductor eddy current loss was accomplished.**

Keywords— large scale electromagnetic field analysis, eddy current, bar-wound coil, permanent magnet synchronous motor .

I. INTRODUCTION

In recent years, in order to solve the serious environmental problems, the automobile industry is actively developing EVs (Electric Vehicles) aiming to realize a zero-emission society. In order to promote popularization in the world in vehicles including large vehicles and city commuters, in addition to improving the energy conversion efficiency of each component of the electric power train, cost reduction and reduction in size and weight are important. In view of these demands, the development of motors using a bar-wound coil (rectangular cross section) has been actively studied for the purpose of miniaturization and high torque density of the motor and improvement of reliability, and it has been put on the market for various purpose [1],[2]. In particular, in the case of the in-vehicle motor, the superiority of the stator design using bar-wound coil is high such as ensuring in-vehicle space due to the improvement of space factor than conventional circular wire inserter type [3],[4]. On the other hand, as a development trend of in-vehicle motors, the development of a technology for improving the power density by increasing the rotation speed is advanced by combining with a reduction gear [1]. Due to the miniaturization and high rotation speed of the motor, not only the iron loss generated by the core material but also the physical phenomena occurring inside the machine, such as conductor eddy current loss caused by the leakage magnetic flux interlinking the bar-wound coil, are complicated [5]. As a result of the above, electromagnetic field analysis as a performance analysis tool of electric equipment requires high resolution analysis results and visualization of loss occurrence place strongly. As a technical trend of improving the iron loss analysis accuracy, in recent years, a play model has been paying attention as one of techniques that can practically model magnetic hysteresis [6],[7]. On the other hand, in the analysis of conductor eddy current loss generated in a bar-wound coil, the calculation scale becomes large when strictly considering the coil end forming portion. Therefore, it takes a lot of calculation time, and it is only simple verification in a two-dimensional model. As far as the author's knowledge, there are few cases where detailed investigation was done due to the above reasons [8],[9]. In recent years, many researches on highly parallel computing using supercomputers have been reported in order to shorten the calculation time of large-scale electromagnetic field analysis. As a previous study, it is evaluated that the speed performance of parallel computing using domain decomposition method by conducting electromagnetic field analysis with large-scale model using super-computer (K-computer in Japan) which can perform massively parallel computation, and the effect of shortening computation time was obtained [10].

In this paper, the conductor eddy current loss is analyzed in detail by the CAE model which strictly modeled the coil and formation in the actual machine of the in-vehicle IPMSM (Interior-Permanent-Magnet Synchronous Motor) by using the calculation method of Ref. [10].

II. ELECTROMAGNETIC FIELD ANALYSIS MODEL

A. Motor Model

Figure 1 shows the motor model and table I show the main specifications. It is an IPMSM with 8 poles and 48 slots (number of phase slots per pole q = 2). In this paper,

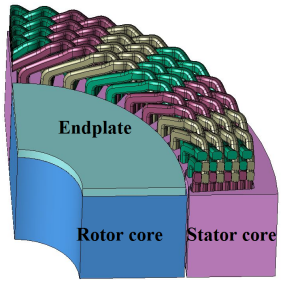

(a) Motor model.

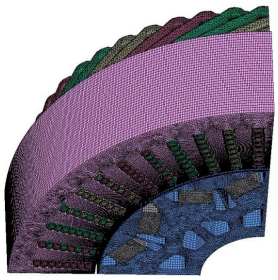

(b) Mesh model without air-region.

(c) Actual machine.

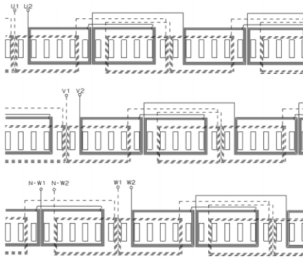

(d) Armature winding pattern.
(Upper: U, Middle: V, Lower: W)

Fig. 1. IPMSM model.

Table I. Specifications of prototype.

Number of rotor poles	8
Number of stator slots	48
Stator core outer diameter	125 mm
Air-gap length	0.6 mm
Axial length of core	51.8 mm
Maximum rotation speed	15,000 r/min
Maximum torque / output	30 Nm, 10 kW
Maximum armature current	150 A_{rms}(Maximum), 75 A_{rms} (Rated)
Cooling method	Water cooling
Number of armature coil-turn	8 turn / slot
Armature winding connection	4 series - 2 parallel
Conductor cross section	4.2 mm^2 / coil
Core material	35H-EA (Nippon Steel & Sumitomo metal)
Magnet material	N48TS-GR (Shinetsu chemical)
Endplate material	SUS304 (thickness: 2.5 mm)

electromagnetic field analysis is carried out with a sinusoidal current source at three main driving points in Table II. Here, the magnetic pole position defines the position where the N-pole of the PM (Permanent Magnet) -rotor faces the U-phase armature winding direction at the +*d*-axis, the current phase reference is the +*q*-axis, and the -*d*-axis is the advance angle direction. The conductor size without the insulation coating of the rectangular copper wire is 1.6 mm * 2.7 mm and the space factor is 78.7 %. In order to reduce the torque ripple, the armature winding adopts a two-layer short-pitch winding as shown in Fig. 1 (d). Figure 2 shows the driving characteristics when the actual machine in Fig. 1 (c) is driven under the condition of DC bus voltage of 100-V. As can be seen from this figure, the motor efficiency is lower than that of general

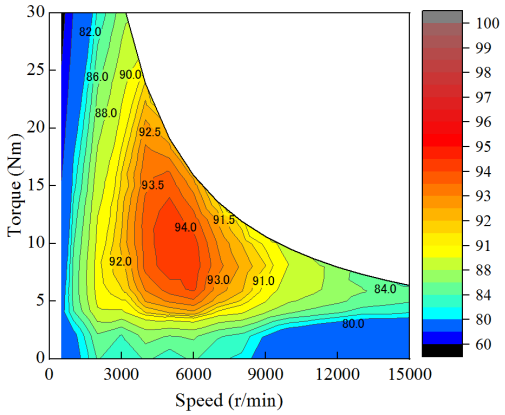

(a) Measured efficiency map in motoring.

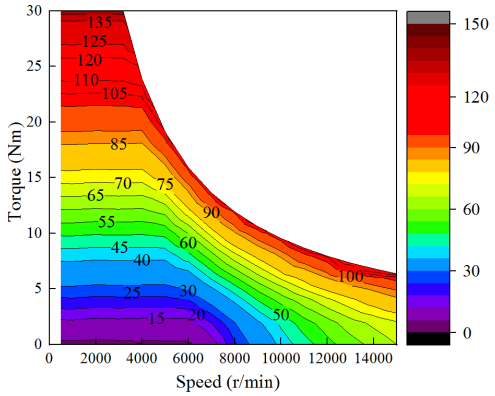

(b) Armature current norm map in motoring.

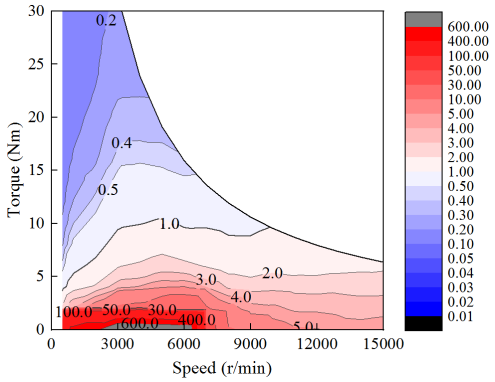

(c) Measured iron loss ratio per copper loss. (W_i/W_c)

Fig. 2. Experimental test results of actual machine.

Table II. Analysis conditions.

Speed (r/min)	Current (A_{rms})	Current phase (deg)
3,183	137.3	44.0
9,000	56.0	73.0
15,000	127.0	81.5

Table III. Measured and analysis results.

Speed (r/min)	Measured (Nm)	FEA (Nm)
3,183	30.0	31.6
9,000	5.0	5.6
15,000	6.9	8.8

IPMSM, because it is compact and designed to have high torque and power density. Figure 2 (b) shows the armature current norm map at each driving point in Fig. 2 (a). Here, the prototype is driven with the MTPA (Maximum Torque Per Ampere) control until the voltage limitation is reached, and under the voltage limitation, it is driven with the current vector that becomes the maximum torque within the voltage limit ellipse. For further consideration, Fig. 2(c) shows the result of mapping the ratio between the iron loss and the copper loss. This figure shows the ratio of the copper loss (W_c) to the iron loss (W_i). When Wi = Wc, the copper loss and the iron loss are equal. On the other hand, $W_i / W_c > 1.0$ is the driving point with a large core loss ratio, and vice versa is the driving point with large copper loss ratio. From this figure, in the low rotation speed and high load region, the low the copper loss is dominant (Wi / Wc < 1.0) because the armature current norm is large, and a result the efficiency is lowered. It is understood that it is necessary to reduce the copper loss by improving the space factor and shortening the circumferential length of the coil. On the other hand, the iron loss is dominant in the low load region. Especially, in this motor model, the efficiency at high rotation speed and low load region is remarkably lowered. This drive region is a region where the iron loss ratio is large from Fig. 2 (c). Because it is a hybrid system with 100-V and a low DC bus voltage, in the high rotation speed range, the current phase is greatly advanced and the field weakening drive is performed, so it is considered that the gap magnetic flux is greatly distorted and the iron loss is greatly increased. On the other hand, since this motor uses a rectangular copper wire with a large cross section, it is considered that the eddy current loss of the conductor is caused by the leakage magnetic flux generated by the field weakening control. However, it is difficult to separate the conductor eddy current loss by actual measurement, and the conductor eddy current loss is included in the iron loss in Fig. 2(c). Especially, in the low voltage hybrid system with applying of this motor, improvement in the motor efficiency at the high rotation speed range greatly contributes to improvement in fuel economy of electric vehicles. Therefore, in the next section, the conductor eddy current loss occurring in the bar-wound coil of the stator is obtained by a large scale calculation using a detailed CAD model.

B. Electromagnetic Field Anaysis Method

In order to obtain an accurate current distribution inside a bar-wound coil, a large-scale three-dimensional mesh model modeled up to the coil end shown in Fig. 1 (b) is used. The number of nodes and the number of elements of the mesh are 1,452,615 and 2,962,666, respectively. In order to shorten the computation time, the parallel computing using domain decomposition method is carried out and K-computer of RIKEN which is capable of massively parallel computation is used [11]. In this calculation, the parallel number is set to 480. In order to separate eddy current loss of the bar-wound coil into conductor eddy current loss and others, electromagnetic analysis is carried out in two ways, i.e., in the case where the current distribution inside the conductor is forcibly made uniform (with out consideration of the conductor eddy current loss, hereinafter referred to as "analysis condition 1") and nonuniformity (with consideration of conductor eddy current loss, hereinafter referred to as "analysis condition 2"). In the analysis condition 1, the current path is calculated beforehand so that the current distribution inside the bar-wound coil is uniform, and in this calculation for obtaining the electromagnetic field distribution, the current density vector inside the bar-wound coil is fixed and the calculated. On the other hand, in analysis condition 2, the current distribution inside the bar-wound coil is obtained simultaneously with the main calculation for finding the electromagnetic field distribution, so the direction and the value of the current vector are influenced by the magnetic flux density distribution interlinking the copper wire. The conductor eddy current loss of the bar-wound coil can be obtained by subtracting the loss of the analysis condition 1 from the analysis condition 2. The iron loss of the core is calculated by a method based on the classical iron loss calculation formula. Since the coefficients of the iron loss calculation formula (eddy current loss coefficient k_e, and hysteresis loss coefficients k_h) have magnetic flux density and frequency dependence characteristics, each coefficient value is referred to from the frequency and magnetic flux density value obtained by discrete Fourier transform of the magnetic flux density distribution obtained by electromagnetic field analysis. Then, the iron loss is calculated for each element unit of the mesh. The coefficient value of the iron loss calculation formula is calculated from the iron loss result of the experimental test results using the ring sample and the eddy current loss coefficient k_e is set to a value of 0.15 ~ 0.75 depending on the reference magnetic flux density value and frequency. The value of 51.2 ~ 243.2 was used for the hysteresis loss coefficient k_h according to the magnetic flux density to be referred to.

III. Electromagnetic Field Analysis Results

A. Torque Analysis Accuracy

Table III shows the result of comparing the measured value with the calculated torque by the analysis method in Section II-B. In the table, at 15,000 r/min, there is a difference between the analysis and the measurement result. The analysis is performed with a sinusoidal current source, but since the actual machine is driven by rectangular voltage control, it seems that loss due to time harmonic is not recorded. Detailed electromagnetic field analysis considering time harmonics will be reported near the future as the future work.

B. Leakage Flux Distribution

At each driving point in Table II, at 3,183 r/min, it is the base speed, and it is driven under MTPA point. Since it is driven within the voltage limit under the flux weakening region at 9,000 r/min and 15,000 r/min, the current phase is advanced. As a result, it can be confirmed that the three-dimensional leakage magnetic flux increases as the rotation speed increases, as shown in Fig. 3. As the current phase advances, the magnet flux vector and the armature magnetic flux vector are opposed, so that the magnet flux tends to leak in the axial direction. In the Fig. 2, leakage magnetic flux is generated not only in the rotor but also in the stator. When this leakage magnetic flux interlinks with the conductor, eddy currents flow in the conductor and conductor eddy current loss occurs. The current

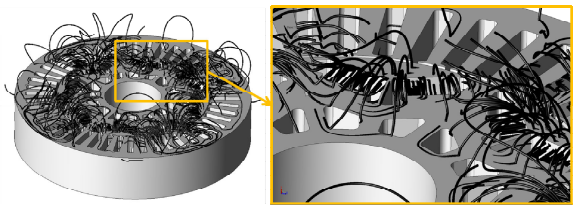

(a) 3,183 r/min.

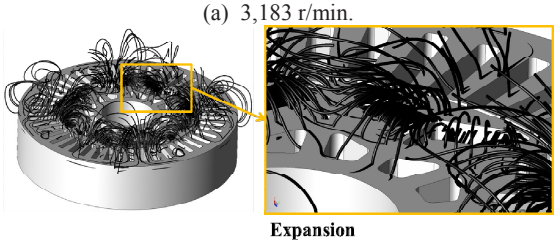

(b) 9,000 r/min.

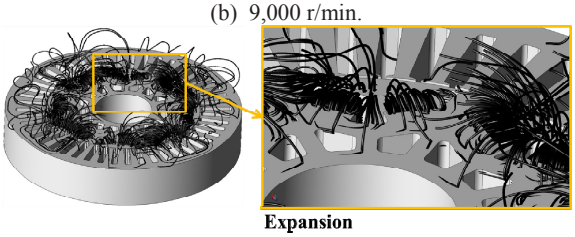

(c) 15,000 r/min.

Fig. 3. Three-dimensional magnetic flux lines.

density distribution in the coil is visualized and evaluated in the next section.

C. Current Density Distribution of Bar-Wound Coil

The current density distribution of the coil contributing to the conductor eddy current loss was obtained by differentiating the analysis condition 1 from the analysis condition 2 using the "result difference function" of electromagnetic field analysis software (JMAG-Designer, developed by JSOL corporation) and visualized results are shown in Fig. 4. In the same drawing, a radial sectional view is also shown at each rotation speed in order to grasp the eddy current distribution of the conductor in the coil end portion and the slot. It can be confirmed from the figure that at 3,183 r/min of the constant torque drive, the conductor eddy current distribution concentrates in the slot inner field, particularly the coil near the air-gap. It is considered that leakage magnetic flux that short-circuits between the stator teeth are caused by linkage with the conductor. On the other hand, it can be confirmed that the conductor eddy current distribution occurs also in the coil end portion at 9,000 r/min and 15,000 r/min in the flux weakening region. As shown in Fig. 3, as the current phase advances, the armature magnetic flux vector and the magnet flux vector faces each other, and as a result, the amount of magnetic flux leaked spatially in the axial direction is increased. Then, it is considered that the conductor eddy current is generated at the coil end portion by the leakage flux linking with the coil end portion. Furthermore, it can be confirmed that the conductor eddy current is generated in the coil on the stator outer diameter side as compared with the case of 3,183 r/min. It is

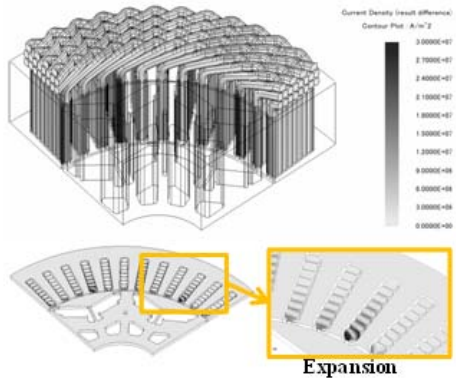

(a) 3,183 r/min.

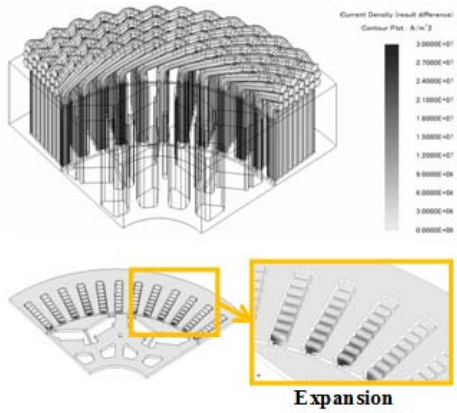

(b) 9,000 r/min.

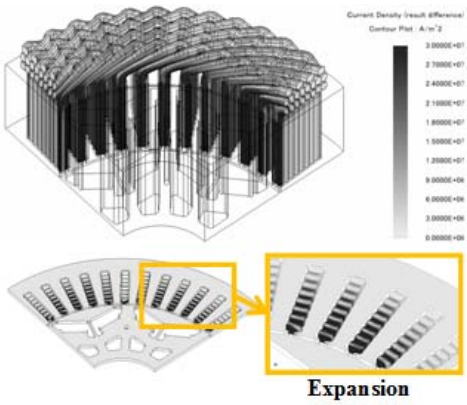

(c) 15,000 r/min.

Fig. 4. Conductor eddy current density distribution.

thought that this is due to the fact that the amount of magnetic flux short-circuiting the inside of the stator tooth is increased by flux weakening control.

D. Breakdown of Conductor Joule Loss

The eddy current loss generated by the eddy current distribution visualized in the previous section is numerically grasped in this section. In order to investigate future eddy current loss countermeasures, eddy current loss in the slot and eddy current loss in the coil end portion are separated. Figure 5

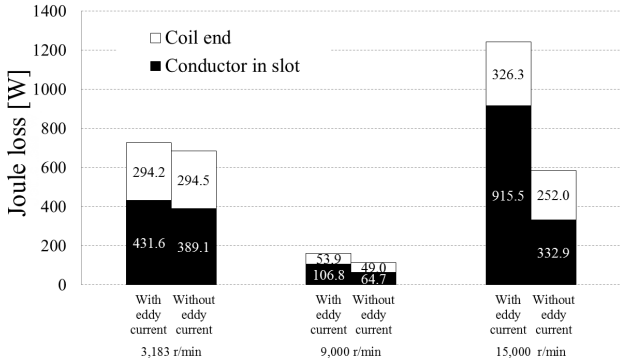

Fig. 5. Breakdown of conductor Joule loss.

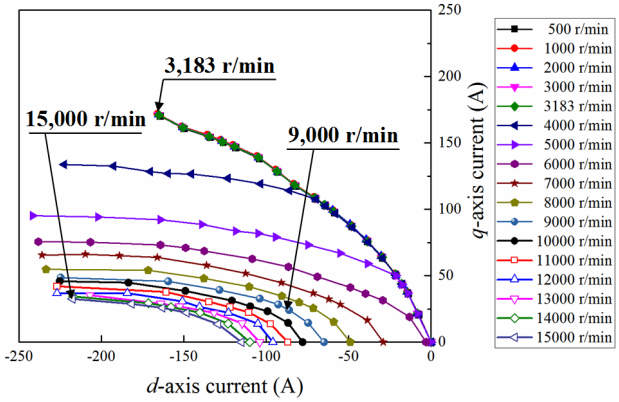

Fig. 6. Armature current vector trajectory.

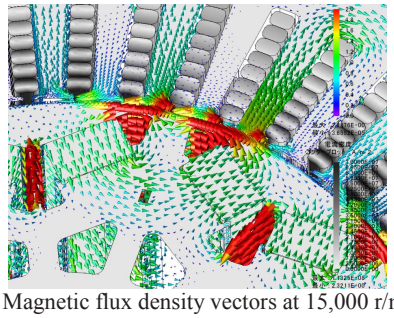

(a) Magnetic flux density vectors at 15,000 r/min.

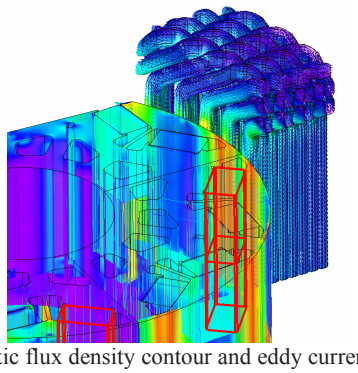

(b) Magnetic flux density contour and eddy current vectors in bar-wound armature windings at 15,000 r/min.

Fig. 7. FEA analysis results at 15,000 r/min.

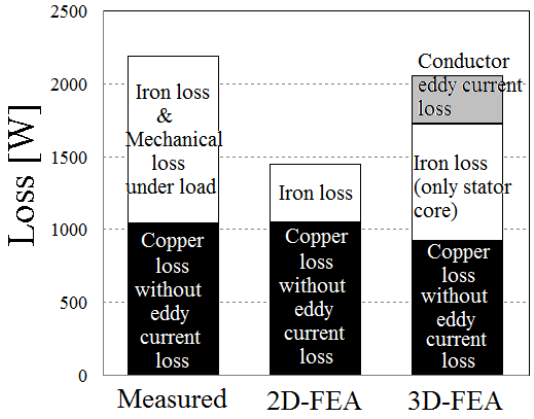

Fig. 8. Loss analysis at 15,000 r/min.

shows the breakdown of conductor Joule loss. From this figure, it can be confirmed that the conductor loss in the armature winding is increased by generating the conductor eddy current loss at each driving point. Due to conductor eddy current loss, copper loss increased by 106.1 % at 3,183 r/min, copper loss increased by 141.3 % at 9,000 r/min and copper loss by 212.3 % at 15,000 r/min. As the rotation speed increases, the drive frequency increases, so the conductor eddy current loss dramatically increases in the high rotation range. It is seen from the figure that the eddy current loss in the conductor in the slot is more conspicuous that the conductor eddy current loss in the coil end portion generated by three-dimensional leakage magnetic flux. The contribution of copper loss in the conductor in the slot and the conductor in the coil end part as a result of considering the conductor eddy current loss is evaluated by using the copper loss of the coil end part as a denominator and the copper loss in the slot as a numerator, as follows. 146.7 % at 3,183 r/min, 198.1 % at 9,000 r/min, and 280.6 % at 15,000 r/min, respectively. Figure 6 shows the armature current vector trajectory with respect to rotation speed and load condition. Figure 7 shows the magnetic flux density vectors, contour and eddy current vectors in bar-wound armature winding at 15,000 r/min. As shown in Fig. 7, by the flux weakening control, it can be confirmed that the magnet flux vector and the armature magnetic flux vector face each other, and a short-circuit magnetic flux is generated at the tip of the stator tooth. Especially at 15,000 r/min, as the current phase advances greatly as shown in Fig. 6, the gap magnetic flux waveform greatly distorts due to the above-mentioned reason, so that the space harmonic increases. As a result, the conductor eddy current loss is increased.

E. Comparison of Losses

The iron loss calculation was performed by the analysis method in Section II-B. Figure 8 shows the results of comparing iron loss analysis values and measured values at 1,5000 r/min. For the reference, the iron loss results obtained by two-dimensional magnetic field analysis are also included. Here, not that conductor eddy current loss and increment of mechanical loss during loading are included in the measured iron loss. Separation of conductor eddy current loss in actual measurement is a future work. From Fig. 8, the total loss amount is closer to the actual measurement that the result of

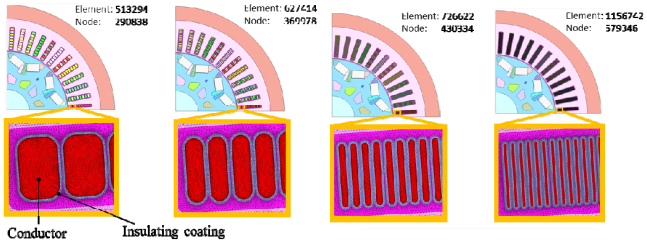

(a) Base. (b) 2-split. (c) 4-split. (d) 6-split.

Fig. 9. Coil-split model in radial-direction.

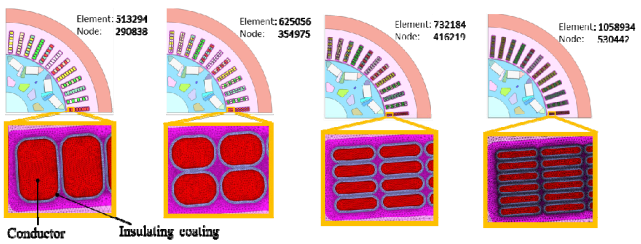

(a) Base. (b) 2-split. (c) 4-split. (d) 6-split.

Fig. 10. Coil-split model in circumferential-direction.

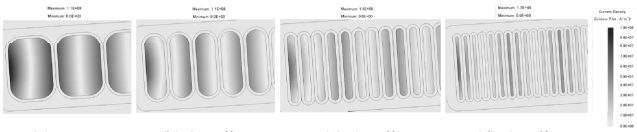

(a) Base. (b) 2-split. (c) 4-split. (d) 6-split.

(a) Base. (b) 2-split. (c) 4-split. (d) 6-split.

Fig. 11. Current density distribution of coil-split model at 15,000 r/min. (Left: radial-direction, Right: circumferential direction)

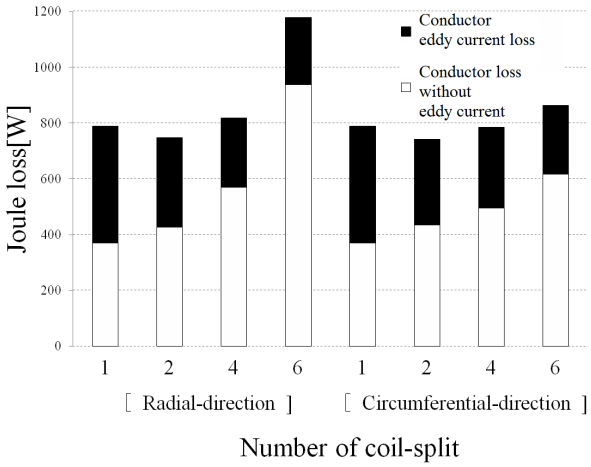

Fig. 12. Joule loss in stator coil.

the two-dimensional analysis by the three-dimensional analysis. In this paper, as a described in Section III-A, although it is analyzed with a sinusoidal current source, when it is at 15,000 r/min of the actual machine, it is region driven by the rectangular voltage control. For this reason, may low order time harmonics are superimposed on the armature current. Since it is predicted that accuracy of iron loss analysis will be improved by considering time harmonics generated by rectangular voltage control, it will be studied in the future. On the other hand, from Fig. 7, the conductor eddy current loss at 15,000 r/min is 16 % of the total loss in the three-dimensional analysis and it can not be ignored. In the next section, the preliminary study of reduction of conductor eddy current loss is implemented.

F. Basic Study on Conductor Eddy Current Loss Reduction

From the results up to the previous section, it became clear that the conductor eddy current loss ratio in the slot is large. In this section, basic investigation of conductor eddy current loss reduction is done by increasing the number of divisions of conductor in the slot. As discussed in the Ref. (8), as a previous study, the eddy current path is shortened, so that the conductor eddy current loss can be reduced. On the other hand, by increasing the number of divisions of the conductor, the conductor resistance increases due to the insulation coating of the conductor, so that it is predicted that if the number of divisions is increased excessively, the copper loss will increase. In this basic study, the relation between the coil division number and the conductor copper loss is clarified by two-dimensional magnetic field analysis when the number of divided conductor divisions is increased in the circumferential direction and/or when the number of divided conductor divisions is increased in the radial direction without changing the insulation coating thickness (0.1 mm). As shown in Fig. 9 and Fig. 10, since there are two kinds of division methods, the number of divisions for base model is changed to 2, 4, and 6 so that the number of parallel connections increased as the number of divisions increased. In this basic study, only the coil division number is changed in consideration of the insulation coating, and the stator core shape was common. Figure 11 shows contour plots of the current density distribution at 15,000 r/min. From this figure, it can be confirmed that the bias of the current density distribution can be reduced by increasing the number of divisions. Figure 12 shows the numerical comparison results of the Joule loss in stator coil. As shown in this figure, by increasing the number of division of coil, the insulation coating ratio increases, the conductor resistance increases and the copper loss increases. On the other hand, the eddy current loss tends to decrease as the eddy current path becomes shorter. From the results of this study, it was found that Joule loss of the conductor can be minimized by dividing the coil into two.

IV. Conclusion

In this paper, the large-scale electromagnetic field analysis of conductor eddy current loss of the stator using a bar-wound coil in IPMSM was studied by using super-computer (K-computer in Japan). In addition, the preliminary investigation of eddy current reduction was attempted. By this research, the eddy current loss distribution at actual coil forming was

visualized, and the loss ratio, i.e., the eddy current loss to the total motor loss, the occurrence of the eddy current in the bar conductor in the slot, or whether it occurs at the coil end portion, was numerically clarified. Furthermore, as a basic study, reduction of conductor eddy current loss was investigated by increasing the number of coil division by two-dimensional analysis.

In the future work, the detailed loss analysis considering rectangular voltage control will be studied and the FE-analysis of investigation of conductor eddy current loss reduction with a more rigorous three-dimensional model will be attempted. Furthermore, the measurement of conductor eddy current loss reduction effect by dividing the bar-wound coil into two-parallel will be indirectly tried from the conductor temperature rise.

ACKNOWLEDGMENT

This research was supported by the Japan Automobile Manufactures Association, Inc., using the Supercomputer "K" of RIKEN. (Grant Number hp170150)

REFERENCES

[1] T. Yashiro, S. Sano, K. Takizawa, and T. Mizutani, "Development of New Motor for Compact-Class Hybrid Vehicle," in *SAE of Japan 2016 International Electric Vehicle Technology Conference Automotive Power Electronics* (*EVTeC* & *APE Japan*), 2016, No. 20169091.

[2] S. Jurkovic, K. Rahman, B. Bae, N. Patel, and P. Savagian, "Next Generation Chevy Volt Electric Machines; Design, Optimization and Control for Performance and Rare-Earth Mitigation," in *IEEE 2016 Energy Conversion Congress and Exposition* (*ECCE*), 2016, pp. 5219-5226.

[3] L. Hao, C. Namudiri, S. Naik, and C. Freitas, "High Speed Performance of PM Machine with Reconfigurable Winding," in *IEEE 2015 Energy Conversion Congress and Exposition* (*ECCE*), 2015, pp. 1840-1848.

[4] S. Jurkovic, K. M. Rahman, P. Savagian, and R. Dawsey, "Electric Traction Motors for Cadillac CT6 Plugin Hybrid-Electric Vehicle," *SAE International Technical Paper*, No. 2016-01-1220.

[5] T. Yamaguchi, K. Ohsaki, and M. Inoue, "Development of New Structure Motor for i-MMD," *IEE-Japan 2017 Industry Applications Society Conference, 2017,* No. 3-54, pp. 267-270. (in Japanese)

[6] T. Matsuo, D. Shimode, Y. Terada, and M. Shimasaki, "Application on Stop and Play Models to the Representation of Magnetic Characteristics of Silicon Steel Sheet," *IEEE Trans. on Magnetics,* 2003, Vol. 39, No. 3, pp. 1361-1364.

[7] T. Matsuo, and M. Shimasaki, "Represenation Theorems for Stop and Play Model with Input-dependent Shape Functions," *IEEE Trans. on Magnetics,* 2004, Vol. 41, No. 5, pp. 1548-1551.

[8] T. Matsuo, and M. Shimasaki, "Represenation Theorems for Stop and Play Model with Input-dependent Shape Functions," *IEEE Trans. on Magnetics,* 2004, Vol. 41, No. 5, pp. 1548-1551.

[9] A. Fatemi, D. M. Ionel, N. A. O. Demerdash, D. A. Saton, R. Wrobel, and Y. C. Chong, "A Computationally Efficient Method for Calculation of Stand Eddy Current Loss in Electric Machines," *IEEE Trans. on Magnetics,* 2012, Vol. 48, No. 7, pp. 2138-2151.

[10] M, Miwa, K. Semba, H. Sano, T. Yamada, Y. Sunayama, Y. Shizawa, A. Azami, and S. Shingu, "A Study of Parallel Supercomputing for a Large-Scale Electromagnetic Analysis on the K-Computer," in *IEE-Japan 2017 Technical Meeting,* SA-17-022, RM-17-022.(in Japanese)

[11] H. Miyazaki, Y. Kusano, N. Shinjou, F. Shoji, M. Yokokawa, and T. Watanabe, "Overview of the K-computer System," FUJITSU Scientific & Technical Journal, Vol. 48, No. 3, pp. 255-265, July, 2012.